Lateral MEMS Microcontact Considerations

Ezekiel J. J. Kruglick, *Student Member, IEEE*, and Kristofer S. J. Pister

***Abstract*— A lateral switching relay structure has been developed which provides a double gold contact with as low as 70-mΩ measured contact resistance, 0.45-A current-carrying ability at MEMS compatible force levels, TTL compatible actuation, and air gap isolation when open. The die area used for the relay mechanism itself (distinct from the actuation) is approximately 75 μm by 100 μm and was designed to allow fabrication of the relays in the MCNC MUMP's dual polysilicon foundry process with no assembly. Design analysis shows that substantial characterization is needed to design optimal microrelays. Temperature softening and failure modes have been characterized by current voltage techniques. Polysilicon vernier structures were used to develop force/current/conductance curves. Relays using thermal actuators have been built. [373]**

***Index Terms*— Contact physics, microrelay, plastic deformation, relay, tribology.**

I. Introduction

MEMS relays have numerous potential applications. The North American relay market alone is U.S. $1.4 billion, and the recent explosive market share of surface mount relays (from 1.2% in 1993 to 19.6% in 1997) demonstrates the value of miniaturization [1]. Additionally, new applications become available as it becomes feasible to integrate large numbers of relays onto smaller substrates. We are targeting several applications such as high-voltage generation which cannot be realized reasonably with solid-state devices due to limited breakdown voltages and electromechanical logic which will be temperature and radiation resistant. The low parasitic feedthrough is an advantage in certain high fidelity applications such as radio frequency (RF) and sensor switching.

For our target applications the most important performance requirements are low drive voltages, truly "micro" size so that large-scale integration is possible, and zero assembly. Impressive previous work has been done using electrostatic[2], [3], [5], [6], magnetic [4], fluid flow [7], and thermal actuation [8], but none meet all three of our requirements.

To define a functional design space for microrelays, appropriate electrodes have been developed and tested and the importance of force, current levels, and materials have been characterized. Our devices have been fabricated in the commercial foundry MUMP's process [10] using a design which does not require assembly.

II. Contact Design

Fig. 1 shows an overview of a lateral relay. The relay is implemented as a crossbar which shorts between two contact points when actuated. Actuation is provided through a supporting frame using thermal actuation [11] or micromanipulators during force characterization. The three beams surrounding the contact points (two behind, one in front between the incoming signals) serve to keep the crossbar planar during actuation.

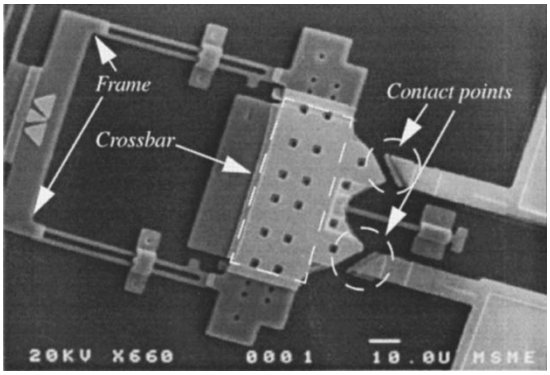

Fig. 1. Scanning electron micrograph overview of the microrelay; scale bar is ten microns. The frame is actuated to close twin contact points, at which point the crossbar shorts between the two inputs (seen at the right edge of the photo).

The MUMPS process [10] has two structural polysilicon layers and a final gold metallization. We want to allow a lateral relay contact design using the gold metallization. Thus an important contact design consideration is the necessity for metal–metal contact. Several lateral contact geometries were tested and the basic types are shown in Figs. 2 and 3. Each contact topology is defined by a vertical (or cross-sectional) and horizontal topology. The basic horizontal topologies are perpendicular contacts, which apply normal contact force, and angled contacts, which approach such that the closure force has both normal and shear components (see Fig. 3). Two different cross-section topologies for bringing gold to gold are shown in Fig. 2. These are classified here as type I and type II.

Angled structures using the type II topology exhibited the best performance. The device shown in the upper right of Fig. 3 exhibits a sub-ohm contact resistance. The contact resistance was stable when cycled by hand over 80 times with a 5-V open circuit, 400-μA load, and forces near 500 μN. Fatigue testing of this sort has been limited by the inevitable eventual mistakes made at a manual probe station. Automatic test structures were thwarted by a layout error.

A direct thermally actuated [11] relay (nonbistable) using the structure in the upper left of Fig. 3 achieved 2.4-Ω contact resistance (for a total relay resistance of 4.8 Ω) and 80-mA current maximum when actuated at 7–12 V. Contacts implemented using the type II angled contacts shown in the upper right of Fig. 3 have conducted 0.45 amps with sub-ohm resistances. These numbers are from cold-switching condition testing.

Manuscript received August 6, 1998; revised May 5, 1999. Subject Editor, K. J. Gabriel.

The authors are with the Sensors and Actuators Center, University of California at Berkeley, Berkeley, CA 94720-1770 USA (e-mail: kruglick@eecs.berkeley.edu).

Publisher Item Identifier S 1057-7157(99)07782-3.

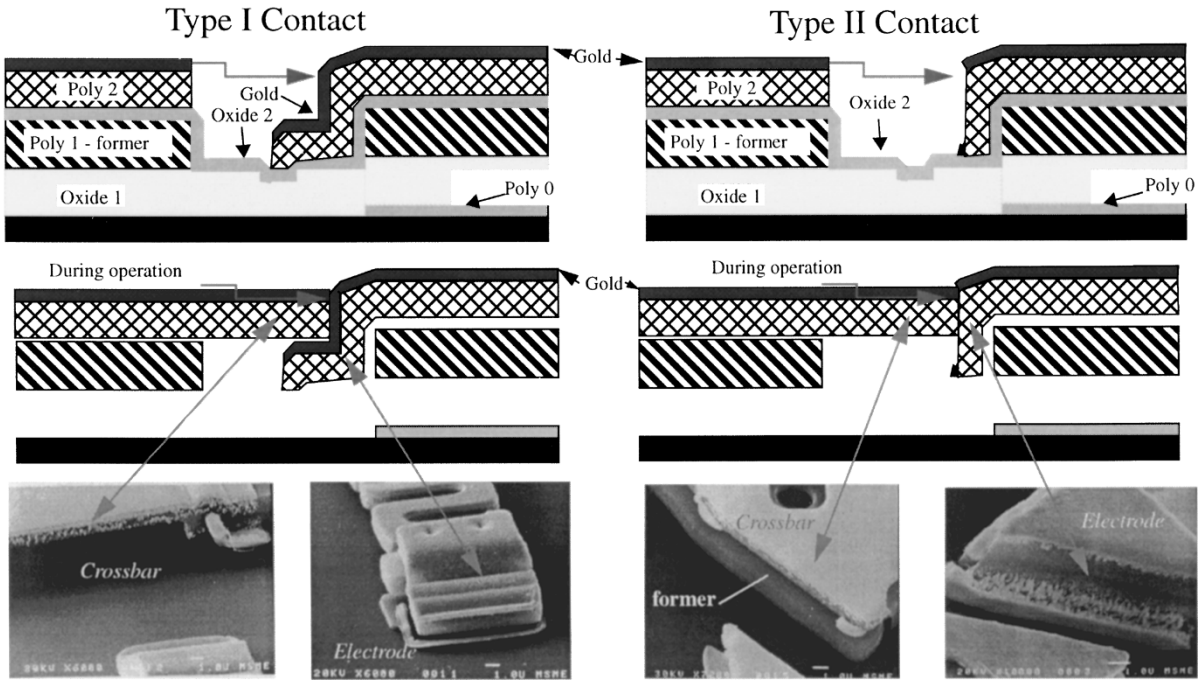

Fig. 2. Two types of lateral contact topologies to attempt gold–gold contact in a polysilicon-based MEMS process. The top line shows a schematic cross section of the designs, with all major material layers labeled. The second line shows a cross section of how each topology is designed to look and function after chemical removal of the oxide layers. At the bottom is a series of SEMS showing the face of the crossbar and electrodes from each design. The left pair of photos are from a contact perpendicular to motion, the right pair are from an angled contact.

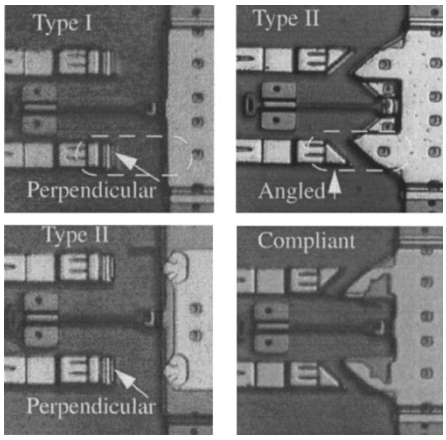

Fig. 3. Views from above of different relay designs. Note that each relay represents two contact points. The areas in the ovals correspond to the areas shown in the SEM's of Fig. 2.

III. Contact Material Issues

The primary consideration for microrelay contact design is contact area. Higher contact area corresponds to lower constriction resistance and lower contact temperature (with correspondingly longer contact lifetime and higher current levels). True contact area and quality at this scale is determined primarily by the force and hardness of the contact material during plastic flow and its resistance to forming surface layers, not by the apparent surface areas brought into contact. The theoretical contact patch between two clean gold surfaces in a 70-mΩ contact has a radius of approximately 127 nm, a negligible part of the overall apparent contact area. Thus the ideal contact material should be both soft and relatively corrosion resistant. Gold, the available metal in the foundry MUMP's process, fits these design criteria quite well.

A second consideration is the adherence force in the relay. The adherence force must be overcome to separate the electrodes and crossbar once contact has been made. The adherence force is a strong function of the mode of operation. As the two contact surfaces come close the first interactions take place at asperities which project above the average surface of the contacts. Initial contact is elastic in nature and has fundamentally derivable electromechanical behavior, however elastic contact has insufficient contact area for reasonable relay performance. As the temperatures increase (softening the material) the surface asperities begin to yield and deform progressively and contact follows "weak" plastic behavior. Weak plastic behavior is more complicated than elastic and is typically characterized by empirical models [13]. As temperature and current densities continue to increase the contact material begins to liquefy and deform destructively and nonrepeatably. This is sometimes referred to as "strong" plastic deformation and is bad for reliability if the contact layers are microscopic, as here. These classifications have been largely empirical and observations from our data suggest that they may simply represent different ratios of the contact being in plastic and elastic regimes. In other words, the physical mechanism is the same but the magnitude of effect is different [24].

The adherence forces measured during elastic behavior in [15] and elsewhere are different for different materials. There are significant differences between hard and soft metals.

The measurements in [16] show that the adhesion forces present after plastic deformation are primarily related to the metal structure. The forces are essentially those required to

tear apart an area of atomically bonded metal the size of the plastically deformed area. Thus the adhesion behavior is related to the crystalline structure and bond formation. Gold forms face centered cubic crystalline structure, which causes the second most adhesion (after tetragonal). However the melting point versus adhesion coefficient of gold is high for a soft metal (see [16, Fig. 22]), which allows for higher current limits.

It has been noted that harder materials such as rhodium show less adherence than gold at comparable force levels [15]. We are not interested in constant force contact design here, but rather comparable contact performance. Rhodium, a typical "hard" face centered cubic contact material, exhibits a higher resistance in the tests where it exhibits low adherence. From basic material properties we see that while gold exhibits 3.6 times the adhesion coefficient [17] rhodium has twice the hardness and twice the resistivity of gold. This predicts very similar behavior for the two materials in a plastic deformation microrelay.

The interrelation of the atomic structure of metals with their adhesion coefficients and hardness leads to the approximation given in [13] that the adhesion force is approximately 40% of the closure force if the separation motion is perpendicular to the surface. This number is commonly considered independent of contact material because it stems from clean metal–metal adhesion in areas where plastic deformation has broken away any surface film. The plastically deformed contact area is inversely related to the material hardness and the tensile strength to pull the contact area apart again is proportional to the hardness [14] so, to first order, the material hardness properties cancel if we assume plastic deformation is reached. Again, this approximation is only appropriate in regimes where the deformation energy is primarily plastic and clean metal contact is broken perpendicularly without significant surface forces. We have not experimentally verified this behavior.

Interestingly, the 40% adherence estimate means that for comparable performance with softer and harder metals the harder metal will have a higher adherence force because it takes more force to reach plastic deformation and low contact resistance. With large forces available in macrorelays, higher adherence forces are irrelevant and harder metals can be chosen for their temperature endurance or arc resistance. Force constrained microrelay design, on the other hand, must place great emphasis on contact and adhesion forces. One of the primary considerations in force limited design, therefore, is what regime of operation we wish to use in the contact: plastic or elastic deformation. Optimal design thus requires extensive contact characterization. We have found that plastic deformation is needed to maximize area for low resistance. This is consistent with most macrorelays, which are also run in the plastic deformation regime. When run in plastic deformation microrelay design favors soft metals for lower adherence at similar resistances.

The overall ramifications are that in a design with relatively large forces, such as most conventional relays, hard metals are an option that can be chosen for the other qualities of the metal. At low force levels such as micronewtons materials issues must be considered carefully with regard to coefficient of adhesion, hardness, and the current and temperature regions of operation for the design.

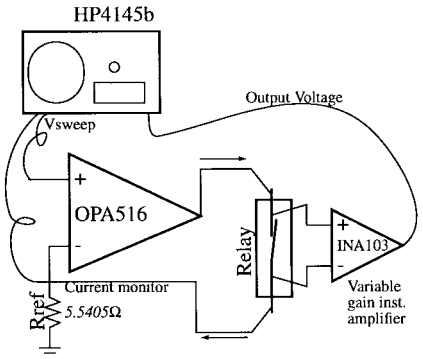

Fig. 4. Extender for high-current high-resolution tests of microrelays. The OPA516 was configured to drive up to 5 A and the instrumentation amplifier was configurable for gains of 1, 10, or 100. Actual gains and offsets were characterized.

IV. Contact Characterization

A. Data Measurement Techniques

Voltage and current were simultaneously measured under computer control by a Hewlett Packard 4145b parameter analyzer. Our 4145b allowed us to drive with a sweep of current from 1 μA to 0.1 A while simultaneously capturing the required voltage up to 5 V. This method was used for most testing at low currents but was limited by our 4145b's voltage resolution of 1 mV and current maximum of 0.1 A.

For higher current range testing an extension setup was built with higher current range and adjustable voltage sensitivity. The higher current range was needed to explore the maxima and modes of failure of the devices. The adjustable voltage sensitivity extended the effective dynamic range of testing by allowing best resolutions on the order of 10 $\mu\Omega$.

The extension takes a swept voltage input from the HP4145b and converts it to current using the circuit shown in Fig. 4. The OPA516 was configured to provide up to 5-A dc current load. The feedback circuit, if ideal, would ensure that the current through the relay was

$$I = \frac{V_{\text{sweep}}}{R_{\text{ref}}} \tag{1}$$

and this was very close to true. However, thorough characterization showed that while the current was very stable and linear at any given relay resistance the exact relation of the current to the sweep voltage varied slightly with load. Thus open loop sweep control was deemed unacceptable and the current was monitored by measuring the voltage across R_{ref}. The resistor R_{ref} was implemented with a temperature stable structure.

The instrumentation amplifier was implemented using an INA103 and was adjustable to have a gain of 1, 10, or 100.

Using this system, four-wire measurements could be made with a voltage resolution of 10 μV while driving up to 5 A. This gives a theoretical single point measurement limit for the system of 1.8 $\mu\Omega$, which can be made better with slope fitting and data averaging techniques. In practice most

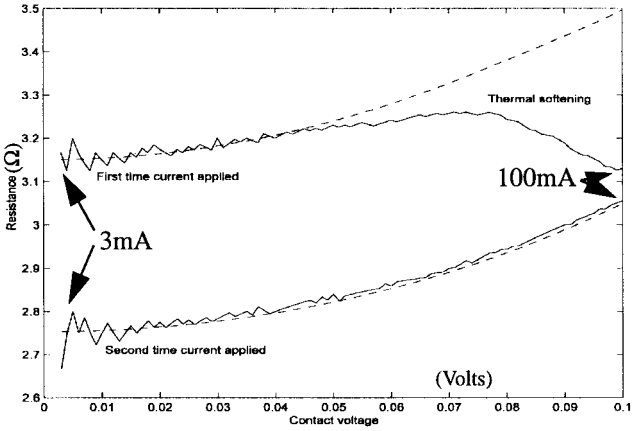

Fig. 5. Theory and measured data for thermal softening on a relay, first, and second current sweep. Expected resistance considering Joule heating but without softening effects are shown as dashed lines. The dashed line from the end of the first data back toward the left is a calculated curve for cooling behavior from the first sweep and heating of the second sweep with constant area and agrees well with the data.

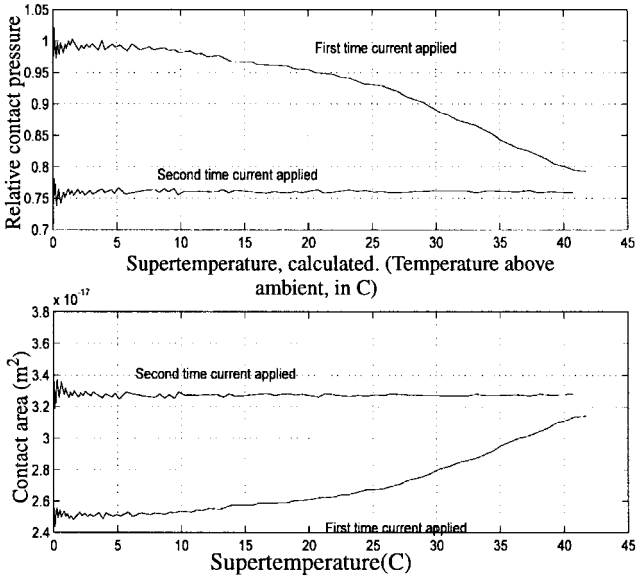

Fig. 6. Plots of calculated effective contact pressure and area for the data of Fig. 5. On the first run the temperature reduces the effective yield pressure, causing the contact area to increase and the contact pressure to decrease. Due to plastic deformation the second run starts with the same contact area as the first run ended with and the contact pressure is below the yielding pressure, even if softening occurs; the second run sees no area change. Temperature above ambient at the contact (supertemperature) is calculated.

measurements were made at lower currents, which reduces the resolution linearly. Most measurements also did not use the maximum amplification so that a wider range of behavior could be observed.

B. Thermal Softening

Fig. 5 shows two plots representing the measured on resistance of a relay on the first and second application of current. The force was applied with a micromanipulator and was held constant, contact was held between current applications. The x-axis has been left in terms of contact voltage in accordance with [13] so that direct behavior comparison can be made. The theoretical performance requires first calculating the temperature at the junction, which was done by dividing the joule heating by the estimated thermal conductance away from the point of contact. The increase of resistance with temperature from [13] is

$$\tau = \frac{R(T)}{R_0} \approx \left[1 + \frac{2}{3}\alpha T\right]. \tag{2}$$

where

- R resistance;
- T "supertemperature" or temperature above ambient at the contact point;
- α temperature coefficient of resistance.

The ratiometric value τ is the change in resistance and is introduced to facilitate calculation of later terms. The results of (2) for a constant area contact are plotted in Fig. 5 as dotted lines. The experimental results match well with theory; the first application of current sees the resistance rise slightly as the temperature increases, then resistance lowers significantly as temperature enhanced mobility softens the contact area—lowering the effective yield pressure. The second application of current follows the predicted thermally induced resistance curve and remains below the resistance of the first run.

The behavior can be seen more explicitly in Fig. 6, which shows plots of calculated area and relative yield pressure from the data of Fig. 5. The area is calculated by using the relation

$$R = \tau\frac{\rho}{\pi b} \tag{3}$$

where ρ is the material resistivity 20.5 nΩ·m and b is the effective radius of the contact spot. When combined with the algebraic area A of a circular contact spot

$$A = \pi b^2 \tag{4}$$

we can calculate the contact area in terms of the raw resistance data

$$A = \frac{1}{\pi}\left(\frac{\tau\rho}{R}\right)^2. \tag{5}$$

From this area the relative contact pressure is directly calculated under the assumption that the force during the test was constant. Since the relay was in a known plastic regime the contact pressure is approximately the yield pressure and the lower contact pressure shows thermal softening.

The contact area is seen to change under constant contact load during the first current sweep as the material softening lowers the yield pressure. This illustrates the earlier point that contact area in a microcontact is explicitly dependent on the applied force and the hardness of the material. The dependence is illustrated by the relation for the area of a purely plastic contact [13]

$$F = AHn \tag{6}$$

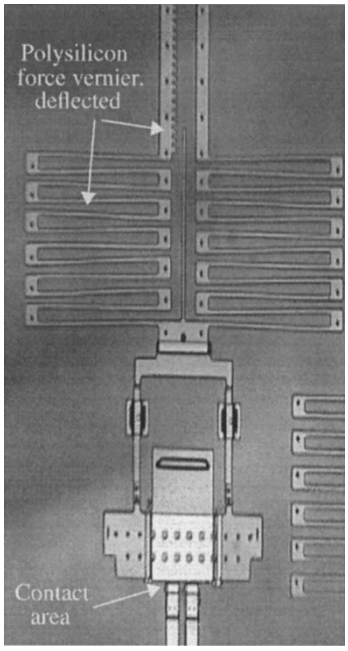

Fig. 7. Crossbar on polysilicon vernier to allow measurement of force during I–V contact characterization. Deflection of vernier is converted to force through linear beam theory.

where

- F applied force;
- H hardness of the material expressed as universal hardness (units of force per area);
- n empirical factor which varies by material and preparation but tends toward an ideal value of one on clean and smooth samples.

After the first current cycle, the second cycle starts out with the plastically deformed contact area from the first run, noticeable in Fig. 5 as the difference in low current resistance. The second run then experiences less Joule heating than the first as well, due to the decreased resistance, and never reaches the softening point which would be required to cause further plastic deformation. Not much temperature increase is needed (increase of 20–30°C) to promote thermal mobility induced softening of the work hardened microstrain area around the contact [13].

C. Force/Current/Conductance Characterization

To characterize the type I contacts shown in Fig. 3 we designed structures supporting a crossbar on a vernier with a predictable spring constant as in [18] (Fig. 7). The structure was pushed into contact using probes and the force was measured by measuring the displacement of the vernier springs on a video screen. The resolution of the system is 0.1 μN after magnification, measurement, and calculation. Great care must be taken not to let stiction interfere with the measurements—the vernier is only accurate when all the rovings are deflecting together in a coordinated fashion and the crossbar is sliding freely.

In order to characterize the mechanical mechanisms occurring at various current levels, I–V characteristics were taken at multiple forces and the data was fit to the established relation

$$G \propto aF^b. \tag{7}$$

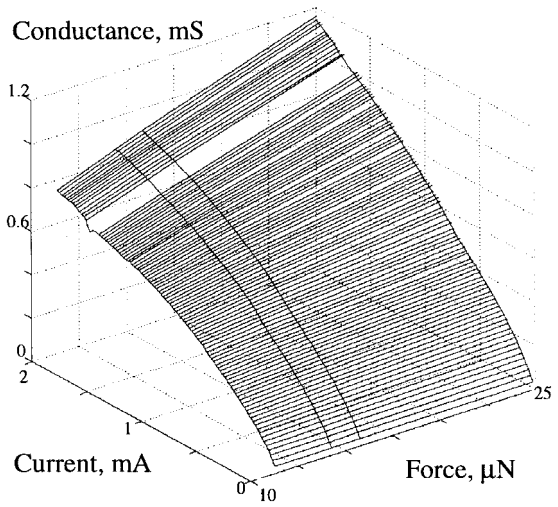

Fig. 8. Conductance versus force and current. Current is a factor because of temperature. Equicurrent lines represent model fits to (7). Data was not fitted for a group of four points where the data at the lowest force had bad values.

where

- G conductance;
- a offset;
- b exponential relation between force and conductance.

As surface asperities are forced against each other and electrical contact is made, it can be calculated from basic principles that the conduction area goes as force to the 1/3 power during elastic behavior [19]. This means that we expect b to remain at 1/3 during the entire elastic regime. The exponent b has been approximated [13] as 0.5 during plastic deformation and unity when resistance is dominated by surface contamination. Current, conductance, and force data is shown in Fig. 8. The first point gives a and fitting the shape of all the points gives b (Fig. 9). We expect the equicurrent fits to show different values of b as the gold contact asperities soften with temperature, similar to the behavior observed in the previous section. If the experiment behaves according to theoretical ideals we should observe an initial plateau at $b = 1/3$. The value of b should then undergo some sort of transition toward a value of 1/2, eventually ending up at some value from 1/2 to 1 depending on the condition of the surface.

The resulting values of b from the data fits are shown in Fig. 10. The expected elastic region (region I, $b = 1/3$) is clearly visible. At a certain current (and associated temperature) the value of b begins to increase again, signaling a transition toward the expected value for plastic yielding (region II). As the current continues to increase the value of b begins to change more slowly and tends toward a limit which may represent a combination of surface films and plastic behavior. Earlier publication that region III models were less statistically significant [20] were based on a mathematical error. The initial rise to 1/3 in Fig. 10 contains statistically very significant models but is not well understood. Previous work has indicated that at extremely small deformation levels

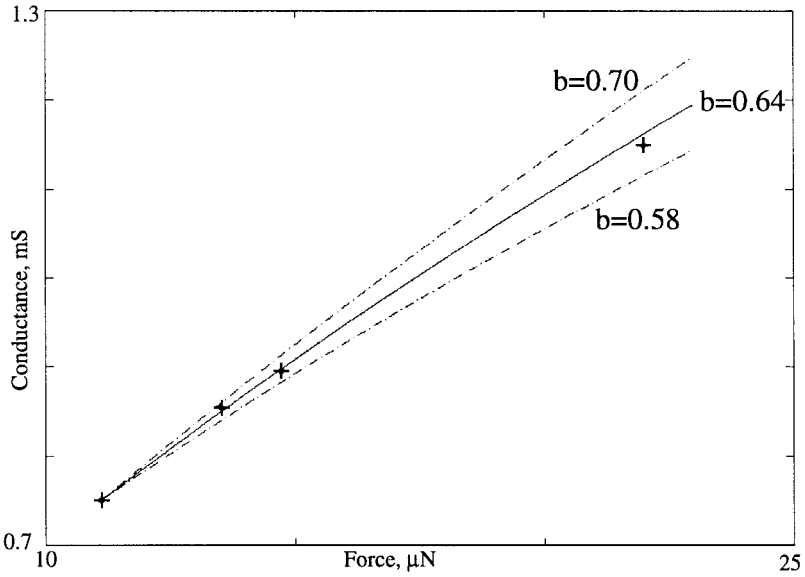

Fig. 9. A single conductance versus force line from the previous figure, showing that changes of 10% to the exponent produce curves that diverge strongly from the observed behavior. Each conductance versus force line was fit to find the exponent, b.

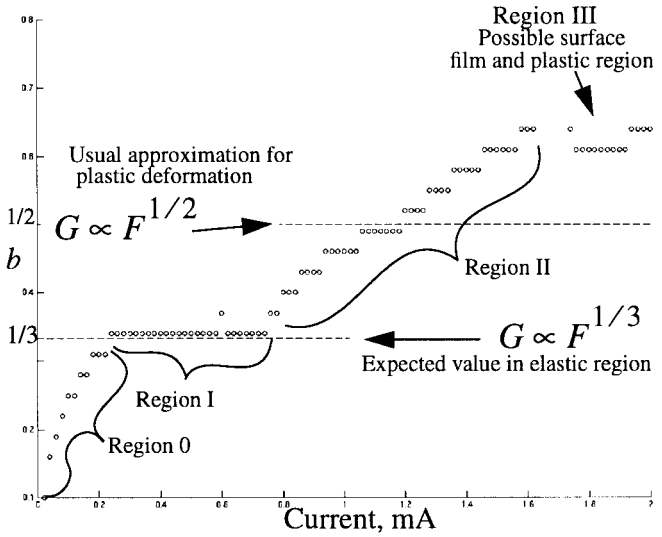

Fig. 10. Plot of the fitting constant b for lines of equal current in Fig. 8. Uncertainties for the value of b are 0.015. This shows strong experimental confirmation of some expected behavior.

the Young's modulus of gold increases by a factor of 10 and approaches the ideal crystalline strength [21]. It is possible that region 0 represents transition from this much higher modulus to bulk behavior as previously experimentally observed in nickel [22], but this is still speculation. Currents beyond those shown here caused nonrepeatable degradation in contact behavior for this particular contact geometry and were therefore excluded from this test so that all data could be verified on the same structures. All I–V data sets were taken 100 times and any that did not prove consistent within our error bounds were discarded as unstable. Very good vibration isolation was required.

One possible interpretation of this data is that the structure is undergoing elastic behavior at low temperatures, plastic behavior at higher temperatures, and approaching limits due to contaminating films as the softening continues. If this is the case then the transitions from region to region deserve increased scrutiny for understanding the physics of electric contacts. Indeed, preliminary modeling which uses Hertz theory to consider the influence of both a plastic and elastic zone does predict a very similar departure of b from 1/3 above a certain temperature. Similarly, simulations of softening with contaminating films generate similar behavior going from 1/2 to higher b values. However these simulations necessarily still have many fit parameters and cannot be considered rigorous until more experimentation is done.

Also, the data shown in Fig. 8 is now presumed to be polysilicon to gold contact. The absolute magnitude of the resistance can be used to calculate the size of a metal–metal contact area using (3), and if calculated here the result is on the order of picometers. Even if this range were mechanically plausible, the behavior of gold–gold contact becomes mean-free-path limited below 42 nm [23]. Calculations based on a metal–polysilicon contact are more speculative due to the heterogeneous contact but result in more reasonable contact size ranges. New studies are underway to use finer force gradations on gold–gold contacts and collect data from initial current application to clarify these behaviors.

D. Static Thermal Failure

The static current limits were tested by closing contacts and running increasing current through them until burnout. Fig. 11 shows a type I perpendicular contact like that shown in Fig. 1 after being burnt out at 30 μA. Thermal failure over the entire crossbar and electrodes shows that in this static situation the relay undergoes widespread failure.

Similar tests with a type II angled relay required the current extender. The angled type II relay was able to pass 448 mA while remaining below 750 mΩ. The lower resistance (which reduces Joule heating) leads to lower operating temperature in these designs.

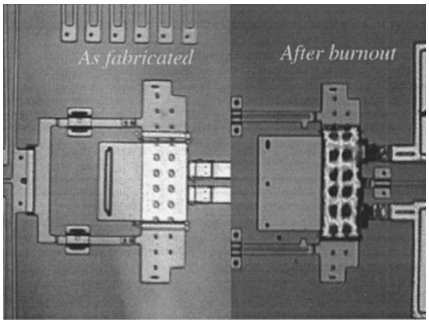

Fig. 11. Type I perpendicular relay test structures as fabricated (left) and after being burnt out with static current (right). All gold on the crossbar shows the effects of melting.

It is possible that enhanced thermal sinking from the crossbar will allow for higher static current loads. By measuring voltage simultaneously as current is increased we were able to view the resistance behavior as thermal failure approached. Behavior showed the expected softening transitions [Fig. 5, eq. (2)] and followed the theoretical thermal response during constant contact area operation.

E. Switching Arc Failure

Examination of the Paschen curve leads us to the expectation that arcing will not be a problem even during hot switching. As the relays close they remain in the nonarc regime and no closing arc is expected. Opening arcs are generated by a different mechanism which still exists in microrelays but are typically quickly quenched and dramatically less destructive than closing arcs. Tens of relays have been operated for thousands of cycles under hot-switching conditions without observed arcs or arc damage. Approximately 20 high-resolution time traces were collected during opening and closing to check for arcs at various voltages from 0.5 to 6 V without observing any detectable arcing. In one case, however, explosive failure was observed in a type II angled relay during closure after several cycles with a current source of 0.1 A (open circuit voltage was 5 V). Transient data was not being collected at the time, so the mechanism cannot be definitely identified.

Fig. 12 shows SEM's of the relay which explosively failed, showing that the failure here was violent and localized. This suggests an arc was responsible. The damage is all within a small area and was sufficient not only to melt metal, as in Fig. 11, but also to blow the top half of the structural polysilicon away [Fig. 12(b)]. Fig. 12(c) shows even more evidence of the localization of the failure—an area of gold which melted and was blown away from the site only to freeze just as suddenly in mid flight. This splash of gold accounts for approximately the same amount of gold missing from its area of origin. The fact that the gold away from the blasted area does not show evidence of melting also emphasizes that this is not static thermal failure, and it may be arcing. It is possible, for example, that a very thin contact bridge was formed by a sharp asperity, sublimated under the current load, and then formed an arc within the resulting metal vapor cloud. The exact mechanism is yet unknown but the data indicates that arcs should not be wholly eliminated from design concerns.

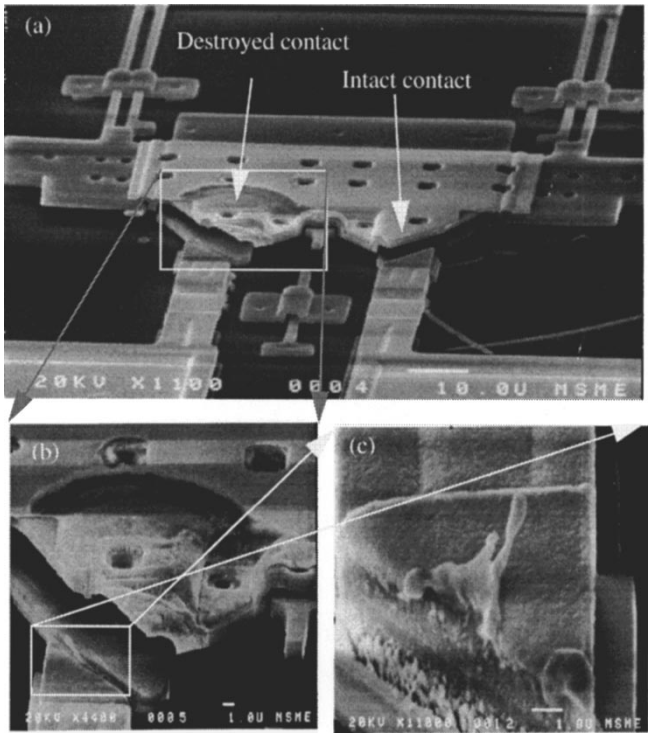

Fig. 12. SEM images of a contact destroyed by sudden discharge, presumably involving arcing. In photo (a) the overview shows both the destroyed contact and its intact neighbor. Photo (b) shows a close-up of the destroyed relay, showing a gouged out area where even the structural polysilicon has been explosively removed. An even closer photo, (c), shows a close-up looking back into the electrode where the destruction occurred. An area of gold has been explosively melted only to freeze again mid-splash. Little or no material appears unaccounted for in (c).

V. Implications for Design

The interrelations of the various design parameters for microrelay design (here largely defined as relay design with extremely constrained force) cannot be overstated. The softer the metal, the less force will be needed to make a good contact which will reduce heating. At the same time high melting temperatures can be desirable for raising the ultimate current limit. Softness, moreover, must be balanced against coefficient of adhesion while basic atomic trends tend to make metals of similar crystal structure more adhesive at lower hardness. Gold is a happy medium for our applications so far as it has low hardness, high melting temperature for a soft metal, and resists surface layer formation.

Some of the cross dependencies result in important feedback during microrelay use. As current and temperature increase the mechanical softening increases the area, in turn reducing the heating and increasing the current carrying capacity. This represents negative feedback for burnout, but increases the adhesion force that will need to be overcome to separate the relays. It is conceivable that at high enough current loads the separation force will have to be stronger than the closure force.

VI. Conclusions

The performance of relays is influenced in several subtle ways by the combination of material hardness, adhesion, and softening temperature. Thermal characterization shows that

temperature effects will do a lot to change the area of contact, thus for adhesion the temperature response and coefficient of adhesion are both important. Additional characterization will be needed for optimization but primary considerations have been established for highly force constrained designs—as opposed to the large force designs of conventional relays.

We have designed several relay topologies and characterized their performance. Optimum performance was about 70 mΩ with 0.45-A current carrying capability. We have characterized thermal response, force performance, and failure mechanisms for these micromachined relays and designed a high-resolution testing system.[1]

ACKNOWLEDGMENT

The authors like to thank R. Wilson for his excellent SEM work and the Hertz Foundation for graduate student support.

REFERENCES

[1] *Semiconductor Business News*, vol. 5, no. 43, Monday, Apr. 14, 1997.
[2] M.-A. Gretillat, Y.-J. Yang, E. S. Hung, V. Rabinovich, G. K. Anantha-suresh, N. F. De Rooij, and S. D. Senturia, "Nonlinear electromechanical behavior of an electrostatic microrelay," in *1997 Int. Conf. Solid-State Sensors and Actuators, (Transducers 97)*, Chicago, June, vol. 2, pp. 1141–1144.
[3] S. Majumder, N. E. McGruer, P. M. Zavracky, G. G. Adams, R. H. Morrison, and J. Krim, "Measurement and modeling of surface micromachined, electrostatically actuated microswitches," in *1997 Int. Conf. Solid-State Sensors and Actuators, (Transducers 97)*, Chicago, June 1997, vol. 2, p. 1145–1148.
[4] W. P. Taylor and M. G. Allen, "Integrated magnetic microrelays: Normally open, normally closed, and multi-pole devices," in *1997 Int. Conf. Solid-State Sensors and Actuators, (Transducers 97)*, Chicago, June, vol. 2, pp. 1149–1152.
[5] I. Schiele, B. Hillerich, F. Kozlowski, and C. Evers, "Micromechanical relay with electrostatic actuation," in *1997 Int. Conf. Solid-State Sensors and Actuators, (Transducers 97)*, Chicago, June, vol. 2, pp. 1165–1168.
[6] H. Schlaak, F. Arndt, and M. Hanke, "Silicon-Microrelay—A small signal relay with electrostatic actuator," in *Proc. 45th Annu. Int. Relay Conf.*, Lake Buena, FL, Apr. 21–23, 1997, paper 10.
[7] J. Simon, S. Saffer, and C.-J. Kim, "A micromechanical relay with a thermally-driven mercury micro-drop" in *IEEE, The 9th Annu. Int. Workshop on Micro Electro Mechanical Systems*, San Diego, CA, Feb. 11–15, 1996, pp. 515–520.
[8] S. Zhou, X.-Q. Sun, and W. N. Carr, "A micro variable inductor chip using MEMS relays" in *1997 Int. Conf. Solid-State Sensors and Actuators, (Transducers 97)*, Chicago, June, vol. 2, pp. 1137–1140.
[9] X.-Q. Sun, K. R. Farmer, and W. N. Carr, "A bistable microrelay based on two-segment multimorph cantilever actuators," in *11th Annual Workshop on Micro Electrical Mechanical Systems*, Heidelberg, Germany, Jan. 25–29, 1998, pp. 154–159.
[10] MEMS Technology Applications Center; 3021 Cornwallis Road; P.O. Box 12889, Research Triangle Park, NC 27709-2889.
[11] J. H. Comtois and V. M. Bright; "Surface micromachined polysilicon thermal actuator arrays and applications," in *Solid-State Sensor and Actuator Workshop*, Hilton Head, SC, 1996, pp. 174–177.
[12] Working Model 2D software, version 4.0, Knowledge Revolution, San Mateo, CA 94402.
[13] R. Holm, *Electric Contacts.* Uppsala, Sweden: Almquist & Wiksells, 1946.
[14] T. H. Courtney, *Mechanical Behavior of Materials.* New York: McGraw Hill, 1990.
[15] J. Schimkat, "Contact materials for microrelays," in *11th Annu. Workshop on Micro Electrical Mechanical Systems*, Heidelberg, Germany, Jan. 25–29, 1998, pp. 190–194.
[16] S. P. Sharma, "Adhesion of electrical contacts," in *22nd National and 3rd Int. Relay Conf.*, Nat. Assoc. Relay Manufacturers, Scottsdale, AZ, 1974, vol. 237, pp. 1/1–14.
[17] S. P. Sharma, "Adhesion coefficients of plated contact materials," *J. Applied Phys.*, vol. 47, no. 8, pp. 3573–3576, Aug. 1976.
[18] R. Yeh and K. S. J. Pister, "Measurement of static friction in mechanical couplings of articulated microrobots" *SPIE Micromachined Devices and Components*, Austin, TX, Oct. 23–24, 1995, vol. 2642, pp. 40–50.
[19] L. D. Landau and E. M. Lifshitz, *Theory of Elasticity.* New York: Pergamon, 1986, p. 31.
[20] E. J. J. Kruglick and K. S. J. Pister, "Bistable MEMS relays and contact characterization," in *1998 Solid State Sensor and Actuator Workshop*, Hilton Head, SC, June 8–11, pp. 333–337.
[21] W. C. Oliver, R. Hutchings, and J. B. Pethica, "Measurements of hardness at indentation depths as low as 20 nanometers," in *Microindentation Techniques in Materials Science and Engineering*, ASTM STP 889, 1986, pp. 7637–7642.
[22] M. D. Pashley and J. B. Pethica, "The role of surface forces in metal-metal contacts," *Journal of Vacuum Science and Technology A (Vacuum, Surfaces, and Films)*, vol. 3, no. 3, pt. 1, pp. 757–761.
[23] J. P. Beale and R. F. W. Pease, "Apparatus for studying ultrasmall contacts" in *Proc. 38th IEEE Holm Conf. Electrical Contacts*, Philadelphia, PA, 1992, vol. 18–21, pp. 45–49.
[24] M. D. Pashley, J. B. Pethica, and D. Tabor, "Adhesion and micromechanical properties of metal surfaces" *Wear*, vol. 100, pp. 7–31, Dec. 1984.

[1] Layout and additional information can be found online at www-bsac.eecs.berkeley.edu.

Ezekiel J. J. Kruglick (S'95), photograph and biography not available at the time of publication.

Kristofer S. J. Pister, photograph and biography not available at the time of publication.